I&EC research
Industrial & Engineering Chemistry Research

Article

Cite This: Ind. Eng. Chem. Res. 2019, 58, 18007−18019

pubs.acs.org/IECR

Mitigation of Iron and Aluminum Powder Deflagrations via Active Explosion Suppression in a 1 m^3 Sphere Vessel

Nicholas S. Reding,*[†,‡] Thomas M. Farrell,[‡] Robert Jackson,[‡] Jérôme Taveau,[‡] and Mark B. Shiflett[†]

[†]Department of Chemical and Petroleum Engineering, University of Kansas, 1450 Jayhawk Blvd, Lawrence, Kansas 66045, United States

[‡]Fike Corporation, Explosion Protection Applications, 704 SW 10th Street, Blue Springs, Missouri 64015, United States

Supporting Information

ABSTRACT: Combustible metal dust explosions continue to present a significant threat to metal handling and refining industries. Addition of noncombustible inert material to combustible dust mixtures, through either premixing or high-rate injection as the incipient flame front begins to develop, is common practice for preventative inhibition or explosion protection via active suppression, respectively. Metal dusts demonstrate an extremely reactive explosion risk due to amplified heat of combustion, burning temperature, flame speed, explosibility parameters (K_{St} and P_{max}), and ignition sensitivity. Inhibition efficiency of suppressant agents used for active mitigation is shown to be reliant on fuel explosibility, discrete burning mechanism, and combustion temperature range and thus may be increasingly variable depending on the fuel in question. For this reason, mitigation of metal powder deflagrations at moderate total suppressed pressures (relative to the overall strength of the enclosure) and at low agent concentrations remains challenging. This paper reviews recent metal dust suppression testing in a Fike Corporation's 1 m^3 sphere combustion chamber and evaluates the efficacy of multiple suppression agents (sodium bicarbonate [SBC], sodium chloride [Met-L-X], and monoammonium phosphate [MAP]) for the mitigation of iron and aluminum powder deflagrations at suspended fuel concentrations of 2250 and 500 g/m^3, respectively.

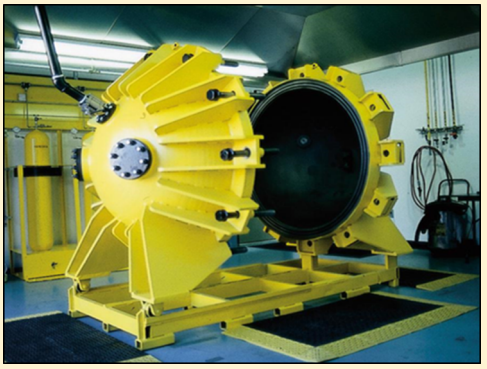

1. INTRODUCTION

Ignition of suspended combustible metal dust clouds remains a serious threat toward personnel and pneumatic conveyance equipment within an extensive range of metal refining and processing industries. As reported by a Chemical Safety Board (CSB) investigation on combustible dust hazards, there have been more than 281 combustible dust incidents within the United States between 1980 and 2005, resulting in 119 fatalities and 718 injuries to operating personnel. According to the CSB's tabulation of the occurrences, dusts of metallic nature have accounted for approximately 20% of these 281 explosion incidents.[1] In more recent years, metal dust explosions have continued to exhibit catastrophic intensity. In December 2010, AL Solutions Inc. of New Cumberland, WV, experienced a severe metal dust explosion following frictional heating within a defective zirconium blender unit, ultimately causing three fatalities and one serious injury.[2] Over a 6 month period in 2011, the coupled effects of three separate iron powder flash fires and hydrogen explosions at the Hoeganaes scrap metal processing facility in Gallatin, TN, resulted in five deaths and three injuries.[3] Another considerably more devastating incident occurred at an industrial metal polishing plant in Kunshan, China, in 2014. A succession of consecutive aluminum−alloy explosions led to 146 fatalities, 114 injuries, and 351 million yuan (51 million USD) in direct economic losses.[4]

Development of proper prevention and mitigation solutions for reactive metal powder deflagrations remains challenging. In comparison to organic fuels, metal dust explosion hazards are frequently characterized by increased complexity in their combustion mechanisms, which can often make flame extinction difficult. Metal dust fuels exhibit a notably heightened explosion risk due to their substantial heats of combustion, burning temperatures, flame speeds, ignition sensitivities, and explosibility parameters (maximum rates of pressure rise [K_{St}] and maximum pressure observed in a contained deflagration [P_{max}]). During propagation of a metal dust flame, energy input to the preheat zone is driven by a greater degree of radiative heat transfer, in addition to standard conduction and convection pathways, which leads to a more substantial flame proliferation rate and explains the amplified spontaneity commonly associated with metal powder combustion.[5−7]

Solids processing industries typically introduce an inert material to combustible dust through two principal methods, preventative inerting or deflagration mitigation following ignition. The first approach, preventative inerting, consists of

Received: July 24, 2019
Revised: August 22, 2019
Accepted: August 27, 2019
Published: August 27, 2019

DOI: 10.1021/acs.iecr.9b04021
Ind. Eng. Chem. Res. 2019, 58, 18007−18019

premixing an inert additive with the combustible dust such that mixture composition remains below the minimum explosible concentration (MEC) of the fuel. Two predominant mechanisms are present in this approach: the first is to dilute the combustible materials such that the combustible fraction remains below the MEC, and the second is to provide significant thermal absorption and radiative obscuration to effectively suppress the propagation of the flame front away from the ignition sources. As a result, even if adequate oxygen content and ignition sources are present, combustion will be unable to initiate or propagate. However, this preemptive technique has its shortcomings. Operations must supervise the process closely to ensure that the inertant and fuel are continuously well mixed, which may be challenging if either component is prone to segregation or particle agglomeration. Additionally, if downstream separation of fuel and inert material is not feasible, the customer may not be willing to accept inertant contamination and a lesser grade of product purity.[7]

The second approach, active chemical suppression, consists of the rapid injection of a suppressant agent into the protected volume after ignition of the combustible dust cloud has occurred, with the objective of extinguishing the incipient flame front early in the deflagration development, thereby limiting the explosion pressure below the design strength of the vessel. The key stages of suppression system activation can be summarized as follows: (1) ignition occurs, and the heat of combustion begins to develop pressure within the system. (2) Pressure buildup is detected, triggering high-rate timely injection and complete dispersion of a suppressant agent into the protected volume. (3) The suppressant agent absorbs heat from the developing combustion, quenching the flame front and limiting further pressure growth. Once released into the enclosure, the suppressant agent has primary functions of absorbing heat generated by the emergent explosion and of inerting the unburnt region of the suspended dust cloud.

Current design techniques for reactive metal deflagration suppression rely predominantly on physical heat absorption properties of the inert material. For industrial applications requiring protection, this suggests the injection of conservatively high concentrations of the suppressant agent into the protected volume, essentially overdesigning the payload of inertant to compensate for the agent's lack of chemical inhibition effectiveness. As investigated by Reding and Shiflett through the thermogravimetric and differential scanning calorimetry analysis of zinc powder oxidation, the overlap of the fuel combustion temperature region and the agent decomposition range seems to allow for increased consumption of free combustion radicals, amplified chemical inhibition effect, and increased heat absorption.[8] A greater degree of overlap results in a kinetically dampened combustion rate and inhibited volatilization of surrounding fuel particles in the preheat zone. Selection of inert materials with increased chemical inhibition could allow for lower agent concentrations required to achieve equivalent total suppressed pressures (TSPs) within the equipment being protected. However, depending on the exact composition of the metal fuel, combustion may occur in different phases (or more than one phase, as in the case of aluminum powder) and at variable temperature ranges. The objective of this study is to investigate the large-scale performance of three agents (SBC, Met-L-X, and MAP) for the suppression of iron and aluminum dust deflagrations, thus potentially enabling the development of more efficient mitigation solutions specifically tailored for certain types of metal fuels.

2. MATERIALS TO BE TESTED

2.1. Suppressant Agents. Suppressant agents sodium bicarbonate (SBC; $NaHCO_3$), sodium chloride (Met-L-X; NaCl), and monoammonium phosphate (MAP; $NH_4H_2PO_4$) have been selected as the suppressant agents to be tested.[9] SBC (CASRN 144-55-8) was acquired from Ansul in the form of "Plus-Fifty C Dry Chemical" (product code 009336), composed of trace amounts of calcium carbonate, attapulgite, and other inert flow-promoting additives. Met-L-X was also acquired from Ansul (product code 009328) and is composed of 80−90% sodium chloride (CASRN 557-04-0), with trace amounts of a heat-absorbent polymer additive, used for desiccation and fluidization of the agent. MAP (CASRN 7722-76-1) was acquired from Amerex in the form of "ABC Dry Chemical Fire Extinguishant" (product code CH555) and contains 90−98% MAP, with trace amounts of inert chemical additives and flow-promoting materials. Decreased particle size yields increased surface area and corresponds to greater inhibition performance of the agent; thus, to eliminate particle size as a potential variable, all suppressant agents were ground and sieved to a similar mean size (20 ± 5 μm). Statistical particle size results and particle size distributions for all suppressant agents are documented within the Supporting Information (Figures C-3−C-5 and Table C-7).

SBC as an agent is prevalent in explosion protection active suppression design. Utilized primarily for the suppression of organic fuel deflagrations, SBC acts as a notable benchmark for comparison. Reported by Taveau et al., 1 m^3 suppression testing on organic dust deflagrations (coal, wheat starch, corn starch) resulted in low reduced pressure (less than 0.3 barg) following system activation at a 35 mbarg pressure detector set point and injection of SBC at 2.3 kg/m^3 concentration. However, the suppression of aluminum dust deflagrations proved increasingly challenging, with total suppressed pressures (TSPs) as high as 2.05 and 0.84 barg at significantly increased SBC concentrations of 4.5 and 9.1 kg/m^3, respectively.[10] For metal dust deflagrations, the TSP is shown to correlate strongly with the suspended fuel concentration. Increased heat liberation and pressure generation over the combustion duration require improved physical inhibition (i.e., greater concentrations of a suppressant agent) to maintain moderate TSPs.

Through 20 L sphere testing, Jiang et al. examined the effects of sodium bicarbonate particle size on the preventative inerting of 5 and 30 μm aluminum dust explosions. Compared to the duration of the SBC inhibition process, the burning time for a single particle of aluminum is relatively brief, and supplementary chemical inhibition modes are too relaxed to effectively impede the flame front. For the mitigation of aluminum combustion, the role of SBC in reducing the fuel burning rate is found to rely primarily on thermal heat absorption mechanisms and oxygen dilution within the preheat zone.[11] This speculated deficiency in chemical inhibition is expected considering the low-temperature decomposition of sodium bicarbonate (see TGA profile for SBC; Figure B-1) relative to the high oxidation temperature range and high maximum adiabatic flame temperature (reported at 3790 °C) of aluminum.[12]

As described by Zalosh, Met-L-X is a certified Class D fire suppressant, commonly utilized in industry for extinguishing a

DOI: 10.1021/acs.iecr.9b04021
Ind. Eng. Chem. Res. 2019, 58, 18007−18019

range of metal hydride fires.[13] NFPA 484 (Standard for Combustible Metals) reports that Met-L-X is the preferred material for the suppression of fires originating from the ignition of the following metals: alkali metals, aluminum, magnesium, niobium, tantalum, titanium, and zirconium.[12] Various other class D agents exhibit similar efficiency in extinguishing the primary metal fire relative to Met-L-X but lack the ability to produce prolonged cooling following the initial event, which allows opportunity for secondary ignition when re-exposed to minimum oxygen content.[13] Thermoplastic polymer additives within the Met-L-X mixture composition impede subsequent diffusion of oxygen to the burning metal by increasing sodium chloride cohesion in the promotion of ample flame coverage. Although it shows prevalence as an effective fire suppression material, sodium chloride has rarely been investigated for use as an explosion suppressant. However, agent decomposition shifted to higher temperatures makes Met-L-X a respectable candidate for aluminum deflagration mitigation due to increased probability for chemical inhibition, as described in Section 2.2.

MAP has been explored for potential as a suppressant agent for metal dust combustion inhibition. During mitigation studies by Jiang et al., the introduction of inert materials SBC and MAP to aluminum powder resulted in irregular flame front upon mixture ignition.[14] In contrast to SBC, MAP at the same concentration exhibited an increased restriction on average flame propagation velocity. Similar conclusions were drawn during experiments measuring the preventative inerting potential of SBC and MAP for the inhibition of 5 μm aluminum dust explosions. MAP was capable of complete aluminum combustion suppression at a minimum inerting concentration (MIC) of 1600 g/m^3, while SBC was unable to prevent fuel combustion at minimum inerting concentrations as high as 2200 g/m^3. Both agents displayed endothermic heat absorption capacity to limit particle volatilization within the preheat zone. However, kinetic modeling of MAP decomposition mechanisms demonstrated an exaggerated competition for oxygen and oxygen radicals when compared to that of SBC, promoting amplified chemical interruption of aluminum oxidation.[14] Chatrathi and Going further investigated the differences between SBC and MAP on the MIC for a variety of fuel types.[15] While both agents demonstrated comparable MIC required to obstruct the expansion of flame front at the ideal concentration of suspended corn starch (625 and 875 g/m^3 for SBC and MAP, respectively), neither suppressant was able to prevent combustion propagation upon the ignition of the optimal concentration of suspended aluminum.[15] Despite some accounts of reported ineffectiveness for the mitigation of aluminum dust explosions, MAP demonstrates promise as a candidate for the suppression of iron powder deflagrations, as described in the subsequent Section 2.2 through the thermogravimetric analysis (TGA) and differential scanning calorimetry (DSC) of iron powder and iron/inhibitor mixtures. Analogous analytical studies on zinc powder combustion directly support claims of amplified chemical inhibition due to alignment of the agent decomposition range with the fuel oxidation temperature range.[8]

Prior to suppression testing on a large scale, appropriate measures were taken to assess the toxicity concerns associated with heating a substantial quantity of metal/inhibitor mixture to high burning temperatures. To appropriately identify the agent decomposition volatiles, TGA-DSC experiments were performed, with evolved gas analysis via mass spectrometry (MS). All samples were measured on the NETZSCH STA 449F1 Jupiter thermal analyzer coupled with the NETZSCH QMS 403 Aeolos mass spectrometer. All MS ion−current curves are shown within the Supporting Information (Appendix D). Such curves for thermal decomposition of SBC under air are displayed in Figure D-1. Evolutions at mass numbers 18 and 44 can be attributed to water (H_2O: MW, 18) and carbon dioxide (CO_2: MW, 44), respectively. Both of these peaks show upmost intensity during the initial decomposition of sodium bicarbonate at approximately 150 °C. Carbon dioxide is evolved at higher temperatures (maximum peak intensity at 669 and 1147 °C) during the secondary decomposition of sodium carbonate. Mass numbers of fragmented ions associated with water (mass number 17) and carbon dioxide (mass number 12) are also present on the MS curve profile. This evolved species analysis aligns directly with the literature-proposed decomposition mechanism shown in eqs E1 and E2 below[8]

$$2NaHCO_{3(s)} \rightarrow Na_2CO_{3(s)} + CO_{2(g)} + H_2O_{(g)} \quad \text{(E1)}$$

$$Na_2CO_{3(s)} \rightarrow CO_{2(g)} + Na_2O_{(s)} \quad \text{(E2)}$$

MS ion−current curves for thermal decomposition of Met-L-X under air are displayed in Figures D-2−D-4. As with SBC decomposition, thermal degradation of Met-L-X releases CO_2 and H_2O, with greatest peak intensity at multiple temperatures below 600 °C. The TGA and associated MS curves for mass numbers 35, 36, 37, and 38 are plotted in Figure D-3. The most probable evolution attributed to these mass numbers is hydrogen chloride (HCl: MW, 36) and its associated fragmented ions. HCl evolution reaches maximum peak intensities at approximately 270 and 1100 °C. The TGA and associated MS curves for mass numbers 70, 72, and 74 are plotted in Figure D-4. The most probable evolution attributed to these mass numbers is chlorine (Cl_2: MW, 70). Chlorine evolution reaches a maximum peak intensity exclusively at the high-temperature degradation region (1100 °C), during which approximately 90% of the sample weight loss occurs.

MS ion−current curves for thermal decomposition of MAP under air are displayed in Figures D-5−D-7. The TGA and associated MS curves for mass numbers 15, 17, 18, and 19 are plotted in Figure D-5. The most probable evolutions attributed to these mass numbers are H_2O and ammonia (NH_3: MW, 17), as well as accompanying fragmented ions, with maximum peak intensities occurring at 215, 350, and 455 °C. The TGA and associated MS curves for mass numbers 30 and 44 are plotted in Figure D-6. The most probable evolutions attributed to these mass numbers are nitric oxide (NO: MW, 30) and nitrous oxide (N_2O: MW, 44), with trace quantities evolving between 200 and 600 °C. The TGA and associated MS curves for mass numbers 35, 36, 48, and 64 are plotted in Figure D-7. The intensities of these evolutions are trivial relative to other evolved species. The mass numbers can likely be attributed to the species HCl and sulfur dioxide (SO_2: MW, 64), as well as the related fragments of these components. Both SO_2 and fragmented ion SO_2 (mass numbers 64 and 48, respectively) show maximum peak intensities at 390 and 475 °C. Both HCl and fragmented ion HCl (mass numbers 36 and 35, respectively) show a slight increase in MS signal intensity above 800 °C. Although monoammonium phosphate contains no single molecules of chlorine or sulfur, it is likely that trace quantities of these evolved species are introduced via thermal degradation of the chemical additives and flow-promoting

DOI: 10.1021/acs.iecr.9b04021
Ind. Eng. Chem. Res. 2019, 58, 18007−18019

materials present within commercially acquired MAP. The mass loss step at approximately 600 °C does not seem to correlate with a particular mass number intensity change, signifying that the evolved species (likely a form of phosphorus oxide based on original sample composition) may have condensed to liquid phase despite a heated transfer line integrating the TGA with the MS. This evolved species analysis can be compared with the literature-proposed decomposition mechanism shown in eqs E3–E5 below[8]

$$NH_4H_2PO_{4(s)} \rightarrow NH_{3(g)} + H_3PO_{4(l)} \quad \text{(E3)}$$

$$4H_3PO_{4(l)} \rightarrow 2H_2O_{(g)} + 2H_4P_2O_{7(l)} \quad \text{(E4)}$$

$$2H_4P_2O_{7(l)} \rightarrow 4H_2O_{(g)} + P_4O_{10(s)} \quad \text{(E5)}$$

With hazards appropriately identified, agents are ready for suppression testing on a large scale using a 1 m^3 combustion sphere. The 1 m^3 combustion sphere is allowed to cool to equilibrium following suppression, and an open exhaust line provides for sufficient venting of potentially harmful fuel and agent decomposition products. To maintain personnel safety, the use of respirators was required for post-test inspection of combustion chamber internals.

2.2. Fuels and Predicted Performances. Based on data of existing explosion protection solutions designed by Fike Corporation between 2015 and 2018, greater than 90% of all metal dust active suppression and/or isolation systems involve either iron (steel) powder or aluminum powder fuels. To satisfy this application demand, pure iron and aluminum powders were thus chosen as the clear candidate fuels for the study. Analysis of alloy-type metals was avoided in this study to prevent misidentification of the fuel combustion range. Additionally, partially oxidized metals were not considered due to the inert tendencies of a metal oxide (limited contribution toward fuel combustion). Both iron powder (Fe-101; CASRN 7439-89-6) and aluminum powder (Al-100; CASRN 7429-90-5) were purchased from Atlantic Equipment Engineers, a division of Micron Metals Inc. Prior to explosibility or suppression testing, mean particle sizes for each metal fuel were determined using laser diffraction particle size analysis (CILAS 990). Statistical particle size results and particle size distributions for both iron and aluminum fuels are provided in the Supporting Information (Figures C-1 and C-2; Table C-6).

When appropriately predicting the efficacy of suppressant materials with an increased affinity toward the mitigation of large-scale flame propagation, two analytical techniques are noteworthy. The first, thermogravimetric analysis (TGA), measures the sample weight change as a function of increasing system temperature. The second, differential scanning calorimetry (DSC), measures the heat flow into or out of the system as a function of increasing temperature. The area beneath a DSC curve indicates the amount of heat released (or absorbed) during exothermic (or endothermic) sample decomposition, which provides an opportunity to quantify the relative capability of compositionally unique inert materials to absorb the heat released as a result of metal powder oxidation and to dampen continued fuel combustion.

The use of a TA Instruments SDT Q600 provided simultaneous TGA and DSC measurements from ambient temperature to a maximum operating temperature of 1500 °C and was used to predict inhibition viability of the suppressant materials considered in this study, as well as to analyze the combustion characteristics of one of the candidate fuels (iron powder). All experiments were performed with ceramic sample pans, under atmospheric pressures, and at a constant heating rate of 10 °C/min. Dust layer thickness for all thermal analytical experiments was maintained below 2 mm to maximize sample exposure to oxygen and to minimize the influence of thermal gradient through the powder. As demonstrated by the iron powder TGA profile in Figure 1,

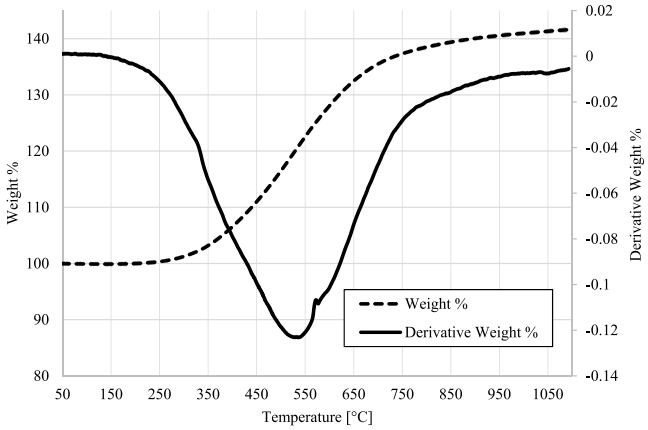

Figure 1. Thermogravimetric profile for iron powder fuel. Temperature range from 50 to 1100 °C, at a constant 10 °C/min heating rate (in air).

sample mass increase due to iron oxidation occurs from approximately 200 to 800 °C (prior to iron's melting point, 1538 °C), verifying that iron is indeed a solid-phase combusting metal.[9]

DSC analysis of iron powder decomposition is overlaid with the DSC analysis of iron/inhibitor mixtures (a 1:1 mixture by mass) in Figure 2a. Integration of DSC heat flow profiles over the iron powder combustion temperature range yielded the total heat release during sample decomposition and was performed via analytical techniques, as illustrated in Figure 2b. Results from the integration of these DSC heat flow signatures are documented in Table 1. Relative to the heat released during iron powder combustion (8640 J/g), the decomposition of the iron/inhibitor mixtures yielded a lower heat release over the temperature range of interest. This consequence is reasonable based on deconstructive interference occurring between exothermic and endothermic heat flow signatures of the fuel and suppressant agent, respectively. The outcome of reduced combustion rate is directly attributable to the degree of physical and chemical inhibitions of the inert material. Releasing only 499 J/g through the iron powder combustion range, the mixture comprising iron powder and MAP exhibited a substantially improved heat absorption efficiency when compared with suppressant agents SBC and Met-L-X. Justification for this increased inhibition efficacy of MAP is hypothesized to be dependent on the extent of overlap between fuel combustion range and the primary decomposition temperature range of the agent. Confirmed through TGA, the majority of MAP sample mass loss occurs from 500 to 750 °C, directly atop the iron powder combustion region (see the TGA profile for MAP; Supporting Information, Figure B-2).[8] Such overlap is theorized to prompt an amplified chemical inhibition effectiveness due to the dilution of oxygen content on the particle surface and increased competition for radical intermediates (·O, ·OH, ·H), which would otherwise

DOI: 10.1021/acs.iecr.9b04021
Ind. Eng. Chem. Res. 2019, 58, 18007−18019

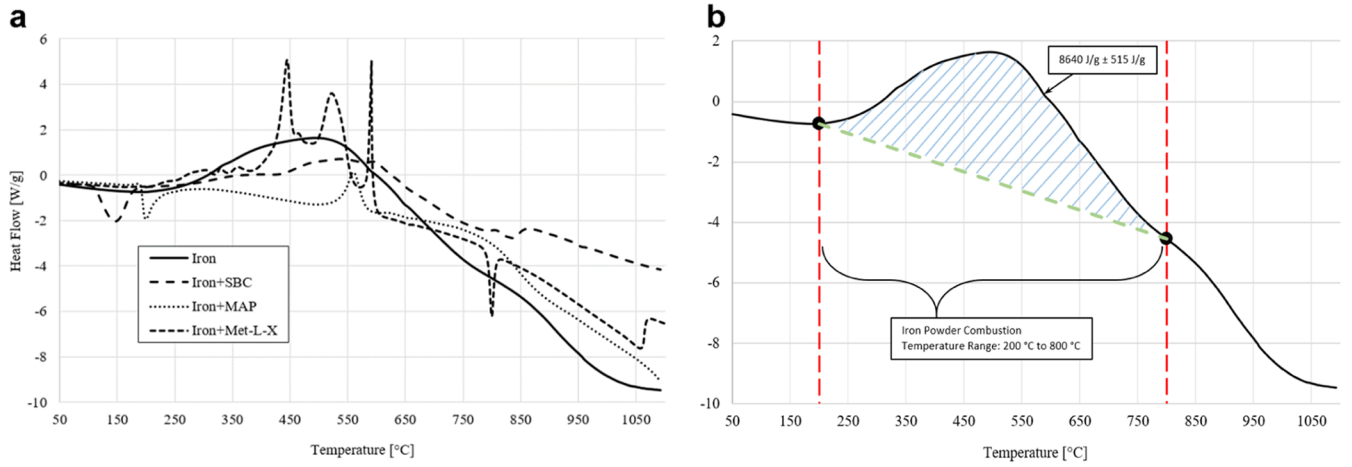

Figure 2. Differential scanning calorimetry profile for iron powder fuel and 1:1 wt % iron/inhibitor mixtures (a), and illustration of DSC integration technique (b). Temperature range from 50 to 1100 °C, at a constant 10 °C/min heating rate (in air).

Table 1. Total Heat Released per Gram of Sample during Decomposition of Iron Powder and Iron/Inhibitor Mixtures; Integration of Figure 2a over the Primary Iron Solid-Phase Combustion Temperature Range (200−800 °C)

sample composition	∑(peak areas within combustion range) [J/g]	average deviation [J/g]
Fe	8640	515
Fe+SBC	4086	29
Fe+MAP	499	48
Fe+Met-L-X	5649	47

stimulate continued fuel combustion, by transient MAP decomposition reaction intermediates (NH_3, $^{\bullet}NH_2$).[8] Primary endothermic agent decomposition of SBC and Met-L-X, however, occurs outside of the iron powder oxidation window, as confirmed through suppressant agent TGA profiles (Supporting Information, Figures B-1 and B-3, respectively), such that the agents are able to operate solely through physical inhibition mechanisms as a result of their solid-state heat capacity and oxygen dilution mechanisms.

Similar techniques for the prediction of suppressant agent performance were not possible for aluminum powder fuel due to the high particle burning temperature. Met-L-X (sodium chloride) decomposes at high temperature in the liquid phase, from approximately 800 to 1000 °C (see the TGA profile for Met-L-X; Supporting Information, Figure B-3), and is hypothesized to exhibit improved flame extinction effects during aluminum deflagrations. The shift of agent decomposition toward temperatures closer to high-temperature aluminum powder combustion offers an increased likelihood for chemical inhibition effectiveness via the introduction of transient sodium and chloride ions. However, such theories were not verifiable through TGA and DSC analysis, as was done with iron powder and iron/inhibitor mixture samples. Figure 3 shows partial TGA/DSC of aluminum powder sample under air, carried out on the NETZSCH STA 449 F5 Jupiter simultaneous analyzer equipped with a SiC furnace capable of operating from 25 to 1600 °C. Primary sample heat release begins within the liquid phase, following the endotherm of melting at 660 °C.[9] The sample exhibited three mass gain steps totaling approximately 71% when heated at a constant 10 °C/min rate. All mass gain rate peaks coincide with DSC exotherm

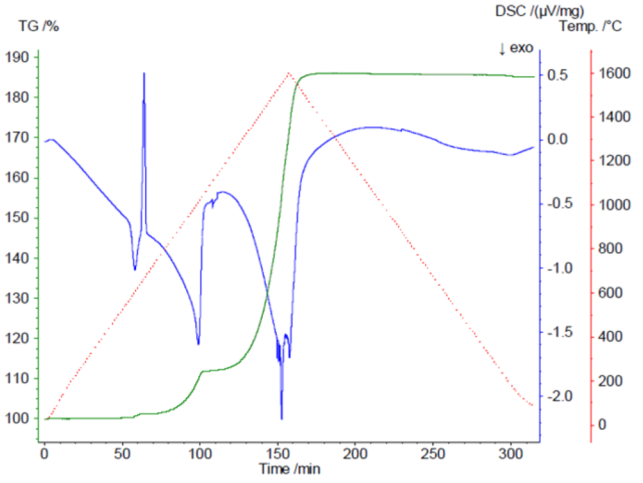

Figure 3. Simultaneous thermogravimetric analysis and differential scanning calorimetry profiles for aluminum powder fuel. Temperature range from 25 to 1600 °C, at a constant 10 °C/min heating rate (in air). Results courtesy of NETZSCH testing facilities.

peaks at 604, 1017, and 1553 °C. However, instrument operation up to only 1600 °C was unable to reveal complete sample oxidation; thus, the analysis of aluminum and inhibitor mixtures would not exhibit useable data since higher-temperature liquid- and vapor-phase exotherms are not visible.

3. EXPERIMENTAL OBJECTIVES AND SETUP

3.1. Open-Air Dispersion. Suppressant materials of different chemical compositions have the potential to exhibit significant variation in physical properties such as cohesiveness, gas permeability, bulk density, compressibility, and floodability. When injected into an open volume under high pressure, these characteristics can often correlate to fluctuating dispersion profiles, flow distributions, and discharge velocities. Before utilizing new inhibitor materials in a contained volume for the mitigation and extinction of developing deflagrations, open-air dispersion testing is necessary to validate the injection performance of all three suppressant agents (SBC, Met-L-X, and MAP). If a particular agent does not meet expectations during suppression testing, it may be difficult to decide whether the cause is limited dispersion during injection or poor inhibition effectiveness. Open-air discharge testing

DOI: 10.1021/acs.iecr.9b04021
Ind. Eng. Chem. Res. 2019, 58, 18007−18019

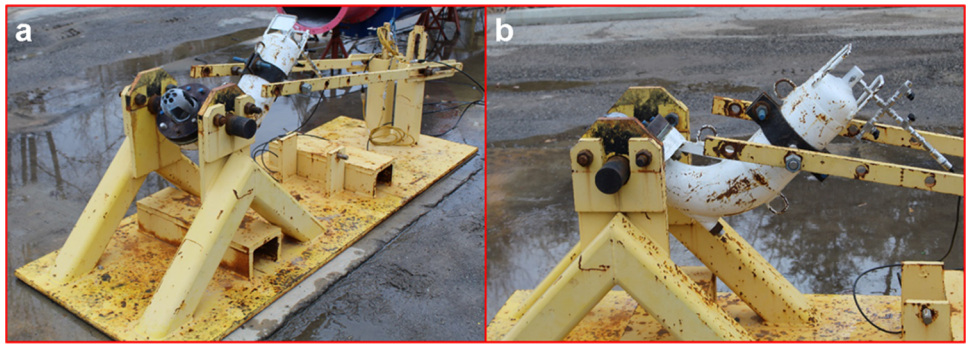

Figure 4. Test setup for open-air dispersion testing, overall setup (a), and container detail (b); a 10 L HRD container with a standard Fike spreader nozzle mounted to the gantry at a 45° firing angle.

beforehand will eliminate such doubts. To fairly evaluate suppression data, open-air dispersion shots are required to ensure that the plume of injected inhibition material behaves similarly for all three agents under analysis, with SBC acting as the benchmark for comparison.

A total of six tests were performed, with two identical tests for each agent to confirm repeatability of discharge performance. A 10 L high-rate discharge (HRD) container was utilized for all experiments to retain a uniform agent delivery rate. To maintain equivalent nitrogen headspace volume in all tests, a constant powder volume of 6.8 L was charged into the container, based on the measured packed densities for all materials (see Supporting Information, Table E-1). These volumes coincide with fill weights of 9.07, 5.90, and 4.08 kg for SBC, Met-L-X, and MAP, respectively. Once loaded with powder and sealed, the HRD container was mounted onto a test gantry at a firing angle of 45° and pressurized with nitrogen to 900 psig (62.1 barg), which served as the primary driving force for high-rate discharge of a suppressant agent through a Fike standard spreader nozzle assembly. The container was equipped with a pressure transducer to measure the vapor space pressure inside the bottle headspace as a function of time following system activation. Vertical and horizontal markers with one-foot spacing increments were positioned in front of the gantry and are necessary when calibrating high-speed experimental software utilized during post-test videography analysis. Initiation of HRD container discharge in all tests was a result of a gas cartridge actuator (GCA) remote firing via a 24 VDC power supply. A visual representation of the experimental mounting setup is shown in Figure 4.

All tests were recorded with a real-time video camera running at 30 frames per second and with a high-speed video camera running at 1000 frames per second. High-speed videography was necessary for post-test analysis. A flashbulb, placed in view of the cameras, was activated at the time of GCA initiation, allowing for the synchronization of data acquisition and high-speed video in the post-test analysis. Using the flashbulb frame as "time zero", reciprocal (inverse) velocity calculations were made at multiple agent throw distances (from origin out to 15 ft) based on data points pulled from high-speed video analysis using the "i-Speed" software suite.

In addition to inverse velocity measurements, data captured from the HRD pressure transducer and qualitative visual inspection subsequent to discharge were necessary for a complete assessment of agent dispersion through comparison of the following post-test deliverables:

- T90, the time required to reduce the nitrogen pressure within the HRD container to 10% of the initial preactuation pressure (90% discharged),
- T03, the time required to reduce the nitrogen pressure within the HRD container to 97% of the initial preactuation pressure (3% discharged),
- Weight of the residual powder left in the container following discharge,
- Confirmation that the rupture disc opening is complete and nonfragmenting, and
- Visual comparison of dispersion profile through the inspection of high-speed videography at specific time frames.

3.2. 1 m^3 Sphere Explosibility and Suppression.

Displayed in Figure 5, the 1 m^3 combustion sphere is a high-strength enclosure (a 21 barg equipment design pressure) composed of two carbon steel hemispherical sections and used primarily for closed-vessel fuel explosibility analysis as per international standard ISO 6184-1 and ASTM E1226.[16,17] The 1 m^3 combustion chamber is capable of being reconfigured with HRD container mounting, a requirement for suppression testing. Ignition energy was consistently provided using two 5 kJ chemical igniters located in the center of the sphere.

Unsuppressed explosibility analysis is essential for the determination of fuel reactivity in the form of maximum observed pressure (P_{max}) and deflagration index (K_{St}), which is proportional to the maximum rate of pressure rise within the contained volume during fuel combustion. At constant ignition

Figure 5. Fike Corporation 1 m^3 combustion test vessel, utilized for fuel explosibility and active suppression testing.

DOI: 10.1021/acs.iecr.9b04021
Ind. Eng. Chem. Res. 2019, 58, 18007−18019

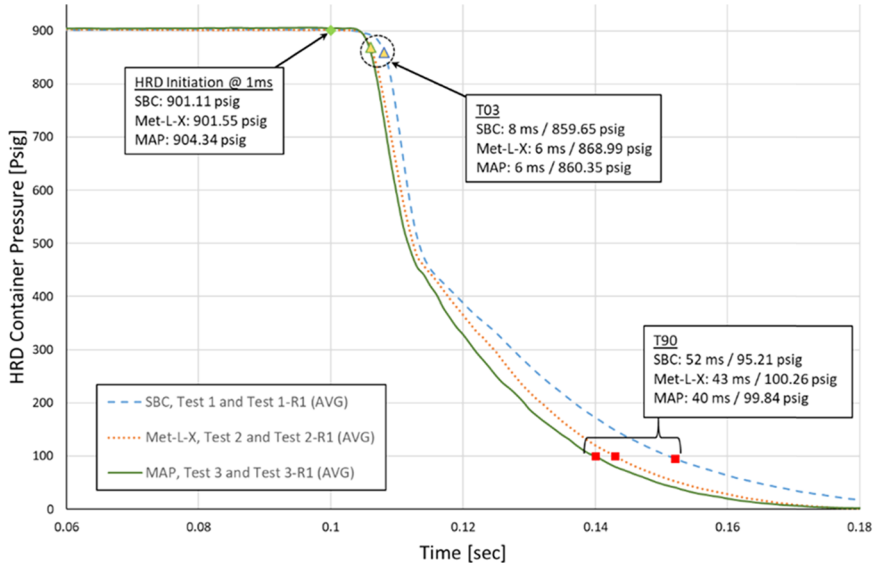

Figure 6. Average container pressure as a function of time following HRD initiation (data reported from t = 0.06 to 0.18 s), acting as a qualitative assessment of T03 and T90 differentiations between tests of varying agent types.

energy and initial pressure, the deflagration reactivity is dependent on the ignition time delay following initiation of fuel dispersion. Reduced ignition time delay induces more aggressive K_{St} due to added effects of turbulence. Increased ignition delay allows turbulence dissipation and a portion of the injected fuel particles to fall out of suspension, leading to suspended concentrations lower than anticipated and resulting in a restricted measurement of K_{St}. Larger concentrations of suspended fuel require dual dispersion (injection via two separate dispersion vessels) to ensure that all fuel is fully injected into the combustion volume prior to ignition, as was the case for all iron deflagration suppression tests performed at an increased suspended fuel concentration of 2250 g/m^3. To guarantee complete injection of fuel, the initial fuel load mass was equally divided among, and simultaneously injected from, each of the two injectors. Fuel injection points were positioned on opposing sides of the 1 m^3 combustion sphere, with dispersion nozzles placed at contrary vertical and horizontal orientations to provide a uniform distribution of fuel.

Active suppression is the process of hindering deflagration propagation by chemically participating in the combustion reaction and/or physically absorbing exothermic heat released from the fuel oxidation. This approach mitigates pressure buildup within the protected volume through the timely injection of a suppressant agent following the onset of ignition. During suppression experiments, full payload of fuel is dispersed into suspension within the contained volume and ignited via a chemical igniter. As the deflagration develops, the resultant pressure growth is monitored. Once the electronic pressure transducer detects that the set point threshold has been reached, the control panel initiates system activation in the form of high-rate suppressant discharge. Nitrogen and suppressant agent are promptly dispersed into the combustion vessel, impeding further expansion of the flame front. The maximum pressure observed within the vessel during a suppressed deflagration event is reported as the total suppressed pressure (TSP). Design of suppression systems for explosion protection applications demands that the TSP be lower than the enclosure strength. All powder loading procedures, HRD container pressurization, and actuation firing mechanism are identical to those described for open-air dispersion testing in Section 3.1.

The TSP acts as a direct indicator of the inhibition performance of the suppressant agent during deflagration mitigation and consists of the following components

$$\mathrm{TSP} = P_{act} + P_{N_2} + P_{comb} \tag{E6}$$

where P_{act} signifies the activation pressure (or set point) of the detector, P_{N_2} represents the pressure due to injection of nitrogen from the HRD container, and P_{comb} indicates the generation of combustion pressure between system activation pressure and complete extinction of the deflagration.

4. DISCUSSION OF RESULTS

4.1. Open-Air Dispersion. The results of this test program act as a necessary supplement toward the continued application of novel agents for metal dust deflagration suppression research. Despite varying flow properties and particulate densities, the dispersion of all three agents appeared visually sufficient to move forward with suppression testing in the 1 m^3 combustion sphere. Although this study was meant to be primarily a qualitative check on the injection proficiency, quantitative deliverables and analysis mentioned in Section 3.1 produced a similar assessment.

Pressure transducer measurements of the container headspace pressure as a function of time allowed for the determination of T03 and T90 for all tests. Discharge of suppressant agents MAP and Met-L-X exhibited a lower T03 (6 ms) compared to that of SBC (8 ms), likely a consequence of variable powder decompression rates. Immediately following rupture disc opening, bridging of compressed powder starts to propagate toward the headspace volume. As the agent packing begins to break apart, interparticulate expansion and expulsion of a bulk agent (as plug flow) promptly follow. Dissimilarities in T03 thus describe differences in the time to effectively fluidize the compressed agent, which is hypothesized to be a function of variable agent particulate densities. Additionally, the average T90 times for MAP and Met-L-X (40 and 43 ms, respectively) were significantly lower than that of SBC (52

DOI: 10.1021/acs.iecr.9b04021
Ind. Eng. Chem. Res. 2019, 58, 18007−18019

Table 2. Post-Test Deliverables for Open-Air Dispersion Testing, Including Measured T90 and T03, Suppressant Weight Left in the Container Following Discharge, and Confirmation of Complete, Nonfragmenting Rupture Disc Opening

test no.	container size	suppressant agent	actual suppressant fill weight (kg)	measured T90 (ms)	measured T03 (ms)	post-test residual powder weight (lbs)	complete and nonfragmenting RD opening (Y/N)
1	10 L HRD	SBC	9.07	52	8	0.054	Y
1-R1	10 L HRD	SBC	9.07	56	8	0.082	Y
2	10 L HRD	Met-L-X	5.90	44	6	0.018	Y
2-R1	10 L HRD	Met-L-X	5.90	46	6	0.036	Y
3	10 L HRD	MAP	4.08	44	6	0.018	Y
3-R1	10 L HRD	MAP	4.08	40	6	0.023	Y

Figure 7. Comparison of plum geometries during open-air discharge testing, including Test No. 1-R1 with SBC (a), Test No. 2 with Met-L-X (b), and Test No. 3 with MAP (c); images captured at 75 ms following system activation.

ms), a direct result of the lesser initial mass charged into the HRD container. The average HRD container pressure as a function of time following HRD initiation is demonstrated in Figure 6 for all three suppressant agents under investigation, with T03 and T90 results for each individual test documented in Table 2.

Qualitative evaluation of plume geometry likewise demonstrates adequate agent dispersion relative to SBC and eases reservations in regard to continued suppression testing. Figure 7 illustrates images captured from high-speed videography at 75 ms following HRD initiation and offers a direct visual comparison of plume distribution for each agent. Plume geometries of SBC and Met-L-X discharges appear nearly identical; all three plume segments are well formed and comparable in extent. The plume for MAP discharge possesses less distinguishable plume segments (rather, identifies as one single cloud) but still covers roughly the same distances at short times following system initiation (increased dispersion lag apparent at larger time/throw). Thus, the high-pressure driving force appears to outweigh differences in agent flow properties such that all agents display similar coverage behavior during discharge.

Figure 8 offers visual depiction of a characteristic cloud profile. Subdivisions of the plume are labeled accordingly as track point 1 (lower segment), track point 2 (middle/primary segment), and track point 3 (upper segment). This nomenclature is essential for data set identification and proper review of inverse velocity data. Annotation lines are also evident, on which data points were collected at 5 ms increments following HRD initiation.

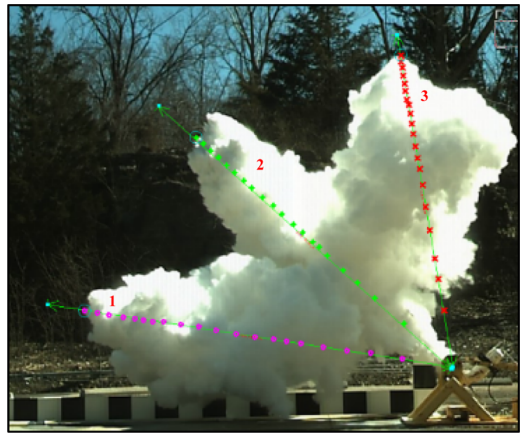

Figure 8. Illustration of dispersion profile during open-air discharge testing (Test No. 2-R1, with Met-L-X powder); subdivisions of the plume (track point 1, track point 2, and track point 3) labeled accordingly in red.

Table E-2 within the Supporting Information displays reciprocal velocity data for the central segment of the cloud profile (track point 2). The values reported are calculated averages of both the original test and the repeat test for the same agent type. Values are provided at arbitrary throw distances of 3, 6, 9, 12, and 15 ft. Inverse velocities were determined with respect to the previous frame (instantaneous inverse velocity) and with respect to the user-defined custom origin position (bulk average inverse velocity). For instantaneous inverse velocity measurements at higher target throw distances, the relative impact of perturbations increases as the

DOI: 10.1021/acs.iecr.9b04021
Ind. Eng. Chem. Res. 2019, 58, 18007−18019

dispersed agent loses momentum and is prone to influence by nonstagnant airflow from the surrounding environment.

The average bulk inverse velocity data with respect to the custom origin is plotted in Figure 9. Results exhibit extremely

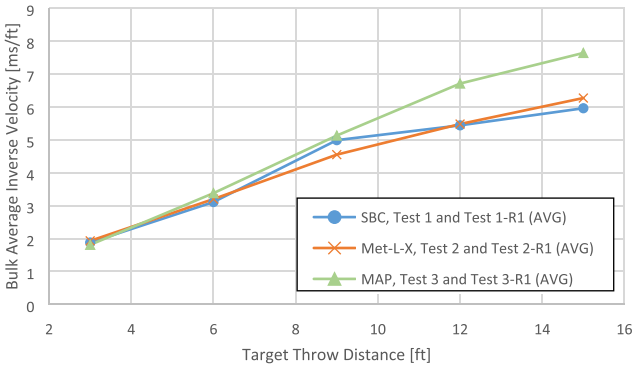

Figure 9. Bulk average inverse velocity results (measured with respect to custom user-defined origin) plotted for all suppressant agents as a function of increasing target throw distance.

similar reciprocal velocities for SBC and Met-L-X. This consistency in inverse velocity between SBC and Met-L-X, even at a larger target throw distance of 15 ft (±0.44 ms/ft), is seemingly due to their comparable particulate crystal densities (2.20 and 2.16 g/cm^3 for SBC and sodium chloride, respectively).[9] As a result of a considerably lower crystal density (1.80 g/cm^3 for MAP), measured inverse velocities for MAP dispersion showed greater deviation from SBC dispersion, more noticeably so at throw distances greater than 9 ft (±1.27 ms/ft at 12 ft and ±1.68 ms/ft at 15 ft). At larger target throw distances, the discharge of MAP coincided with an increased time-to-cover and a limited penetration power, again likely due to the significantly lower particulate density compared to the other agents tested. All aforementioned deviations are based on the average bulk inverse velocity data reported in Table E-2 within the Supporting Information.

Post-test quantification of the residual suppressant weight left in the container was recorded as another auxiliary deliverable and is presented within Table 2. All SBC open-air dispersion tests resulted in >0.05 kg of residual powder left in the container (an average of 0.75% of the initial mass), while all MAP and Met-L-X tests resulted in <0.05 kg of residual powder left in the container (an average of 0.50 and 0.47% of the initial mass, respectively). This minor difference is likely a consequence of lesser agent mass loaded into the HRD initially; the residual mass in the container in all cases is deemed insignificant and injection is considered full and complete.

Photographs of rupture disc opening were taken for all tests as part of post-test documentation. Discharge of all agent types resulted in complete, nonfragmenting rupture disc opening. An illustration of standard rupture disc opening is provided in Figure 10 (Test No. 1-R1; SBC).

Throw distance across the major diameter of the 1 m^3 combustion sphere (to be utilized for suppression testing) is approximately 4.07 ft. Upon review of Figure 9, all three agents display nearly equivalent bulk average inverse velocities at throw distances less than 9 ft, signifying a uniform time-to-cover over this target throw range. In addition to qualitative observations and conclusions drawn from container pressure

Figure 10. Post-test evaluation; validation that HRD rupture disc opening is complete and nonfragmenting; Test No. 1-R1 with SBC.

transducer measurement, this outcome encourages the dependability of upcoming 1 m^3 suppression test results.

Open-air dispersion testing at particular agent fill weights sets restrictions on the structure of the suppression test plan. Discharge performance and agent injection capability have not been validated for container fill weights larger than that which have been tested. Demonstrating the lowest crystal density of all agents tested, the dispersion of MAP at a 4.08 kg fill weight acts as the limiting factor in this regard. During suppression testing, agent concentrations must remain equivalent for proper comparison of inhibition efficacy. All 10 L HRD containers are to be filled with no greater poundage of suppressant agent than was tested in this open-air study.

4.2. 1 m^3 Sphere Explosibility and Suppression. Explosibility testing in the 1 m^3 combustion sphere, as described in Section 3.2, was performed for both iron and aluminum powder fuels prior to suppression testing. K_{St} and P_{max} results, as well as tested fuel concentration and ignition delay, are documented in Table 3. Higher concentrations of fuel were preferable, offering a superior representation of the metal dust flame reactivity. Ignition delay was adjusted accordingly over multiple tests to confirm that the injection and combustion of all fuel were complete. Even at a high concentration of suspended iron, the inspection of dispersion vessels following tests at a 500 ms ignition delay indicated no excess fuel following the event and resulted in no combustion back-pressure through the ball valve. Inspection of the 1 m^3 after each explosibility test at this time delay also exhibited complete combustion of all fuel while in suspension, with no smoldering nests or unburnt fuel on the walls or bottom of the vessel. While this time delay is slightly shorter than that used for standard explosibility testing of typical industrial fuels in this particular vessel (600 ms, calibrated to ASTM standard methods), it was deemed necessary to ensure complete combustion as metal dust fuels inject significantly faster than lower density organics that are commonly used for vessel calibration.

Fuel concentration must also be tuned to ensure that the fuel severity was appropriately demanding of the agents. If the fuel is too aggressive, the agents would be overwhelmed and the deflagration would be unsuppressed. If not challenging enough, it may be difficult to assess deviations in inhibitor performance during suppression testing. At a 2250 g/m^3 fuel concentration, iron explosibility testing yielded an average K_{St} and P_{max} of 61 barg-m/s and 4.52 barg, respectively, while

DOI: 10.1021/acs.iecr.9b04021
Ind. Eng. Chem. Res. 2019, 58, 18007−18019

Table 3. Fuel Particle Size Statistical Analysis and Fuel Explosibility Results via a 1 m^3 Sphere Testing, Presented as the Average of Two Identical Tests

	particle size distribution			1 m^3 explosibility testing			
fuel type	<5 μm	<40 μm	mean size	fuel concentration [g/m^3]	ignition delay [ms]	K_{St} [barg-m/s]	P_{max} [barg]
Al-100	79%	100%	3.51	500	500	170	8.12
Fe-101	11%	76%	26.97	2250	500	61	4.52

Table 4. 1 m^3 Sphere Suppression Test Results for Iron Dust Fuel (Fe-101), with Variable Suppressant Composition

test series	fuel type	fuel concentration [g/m^3]	ignition delay [ms]	suppressant type	suppressant concentration [kg/m^3]	P_{set} [mbarg]	P_{ign} [mbarg]	TSP [barg]
1	Fe-101	2250	500	SBC	4.08 [10 L HRD container x1]	70	1.5	0.59
1-R1	Fe-101	2250	500	SBC	4.08 [10 L HRD container x1]	70	0.7	0.60
2	Fe-101	2250	500	Met-L-X	4.08 [10 L HRD container x1]	70	0.2	0.64
2-R1	Fe-101	2250	500	Met-L-X	4.08 [10 L HRD container x1]	70	5.6	0.60
3	Fe-101	2250	500	MAP	4.08 [10 L HRD container x1]	70	−0.4	0.52
3-R1	Fe-101	2250	500	MAP	4.08 [10 L HRD container x1]	70	1.6	0.50

Table 5. 1 m^3 Sphere Suppression Test Results for Iron Dust Fuel (Al-100), with Variable Suppressant Composition

test series	fuel type	fuel concentration [g/m^3]	ignition delay [ms]	suppressant type	suppressant concentration [kg/m^3]	P_{set} [mbarg]	P_{ign} [mbarg]	TSP [barg]
4	Al-100	500	500	SBC	8.16 [10 L HRD container x1]	35	11.3	1.54
4-R1	Al-100	500	500	SBC	8.16 [10 L HRD container x1]	35	7.4	1.68
5	Al-100	500	500	Met-L-X	8.16 [10 L HRD container x2]	35	3.0	4.95
5-R1	Al-100	500	500	Met-L-X	8.16 [10 L HRD container x2]	35	−5.3	1.85
5-R2	Al-100	500	500	Met-L-X	8.16 [10 L HRD container x2]	35	0.4	1.33
5-R3	Al-100	500	500	Met-L-X	8.16 [10 L HRD container x2]	35	−2.0	1.98
6	Al-100	500	500	MAP	8.16 [10 L HRD container x2]	35	2.9	1.83
6-R1	Al-100	500	500	MAP	8.16 [10 L HRD container x2]	35	−8.2	1.42

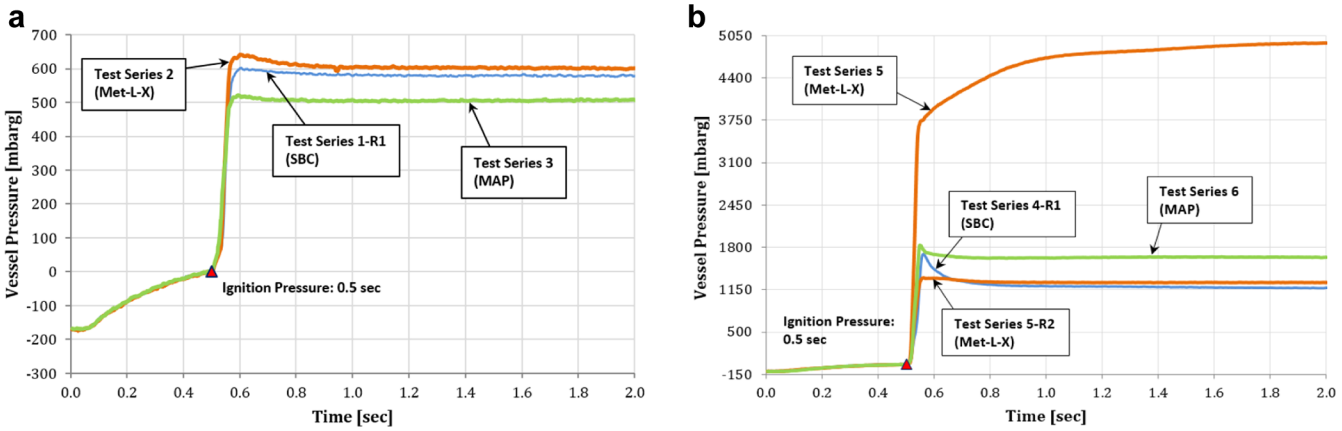

Figure 11. Vessel pressure versus time curves for select active suppression experiments with iron (a) and aluminum (b) powders.

aluminum explosibility testing at only 500 g/m^3 yielded an average K_{St} and P_{max} of 170 barg-m/s and 8.12 barg, respectively. Such an increase in severity at significantly lower fuel concentration reflects the spontaneity and intensity commonly associated with aluminum powder combustion.

Suppression testing in the 1 m^3 combustion sphere was performed on both iron and aluminum deflagrations with the three agents under analysis (SBC, Met-L-X, and MAP). Test conditions and results from this study are documented for iron and aluminum suppression within Tables 4 and 5, respectively. All iron deflagration suppression testing was executed at a 70 mbarg set pressure and atmospheric pressure as the target ignition pressure to allow for moderate deflagration development prior to suppression. Based on agent load constraints from open-air dispersion testing, a constant applied suppressant concentration of 4.08 kg/m^3 required a single 10 L HRD to be utilized for all experiments. Following suppression of iron combustion via injection of SBC and Met-L-X, the analysis of vessel pressure versus time curves (see Figure 11a) yielded effective average TSPs of 0.60 and 0.62 barg, respectively. Suppression with MAP at the same concentration of agent yielded an average effective TSP of 0.51 psig. This reduction can be attributed to chemical inhibition, exploited as a supplement to standard physical inhibition. As discussed in Section 2.2, the thermal analysis of iron and iron and iron/inhibitor mixture samples indicated promising mitigation performance for MAP (which demonstrated nearly 95% reduction in heat released during iron powder combustion) due to amplified degree of overlap between fuel oxidation and primary agent decomposition temperature ranges. Principal

DOI: 10.1021/acs.iecr.9b04021
Ind. Eng. Chem. Res. 2019, 58, 18007−18019

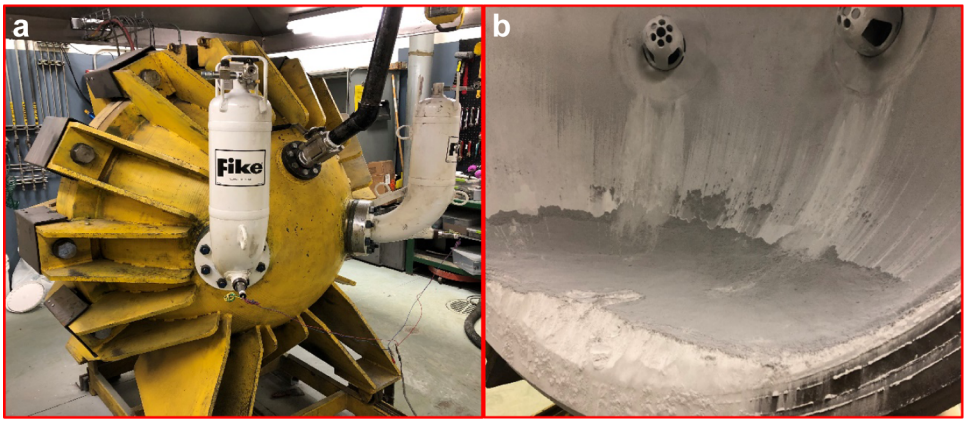

Figure 12. Test setup for a 1 m^3 suppression testing with two 10 L HRDs (a) and residual combustion deposit following active suppression of aluminum deflagration with Met-L-X suppressant agent; Test Series 5 (b).

decomposition of SBC and Met-L-X occurs either before or after the solid-phase iron oxidation range, indicating that these two suppressant agents exhibit roughly the same physical inerting potential and do not function effectively through chemical means for this specific fuel composition.

All aluminum deflagration suppression testing was executed at a relatively lower set pressure of 35 mbarg, atmospheric pressure as the target ignition pressure, and an agent concentration of 8.16 kg/m^3. Compared to applications conveying organic dusts or normally reactive metals, aluminum processing requires protection solutions with significantly lower detection thresholds. In the case of ignition of an extremely reactive metal, prompt system activation allows for the introduction of a suppressant before the deflagration is able to develop energy. Although suppression with SBC required a single 10 L HRD container, suppression with Met-L-X and MAP, both with decreased particulate density relative to SBC, required simultaneous activation of two 10 L HRD containers to maintain a constant suppressant concentration, to retain adequate nitrogen headspace for accelerating the suppression agents during discharge, and to preserve the same time scale for discharge as with SBC (T90). The 1 m^3 combustion chamber setup, equipped with two 10 L HRD containers, is depicted in Figure 12a. Both HRDs were mounted on the same hemispherical section of the combustion sphere, so as to not introduce agent throw distance as a potential variable influencing inhibition performance. Following suppression of aluminum combustion via injection of SBC and MAP, the analysis of vessel pressure versus time curves (see Figure 11b) yielded effective average TSPs of 1.61 and 1.63 barg, respectively. Although complete thermal analytical techniques were not available for aluminum (see Section 2.2), Met-L-X was anticipated to chemically inhibit aluminum combustion due to its high-temperature agent decomposition. However, aluminum deflagration suppression with Met-L-X seemed to demonstrate inconsistent outcomes, with TSPs ranging from 1.33 barg (Test Series 5-R2) to 4.95 barg (Test Series 5). The post-test combustion residue associated with Test Series 5 is shown in Figure 12b. As described in Section 2.1, Met-L-X is primarily composed of sodium chloride and thermoplastic polymer additive used to form a protective layer preventing further diffusion of oxygen to the burning metal surface. Upon inspection of the burnt mixture internal to the combustion chamber, a dark coating was visible atop a partially oxidized fuel and agent mixture. While effective for fire suppression application, the polymer coating appeared to induce a confined smoldering nest when employed for explosion suppression. Continued partial combustion of unsuspended fuel allowed for a steady build of pressure until the end of data collection approximately 1500 ms after the initial ignition of fuel. As long as bulk flow properties are not compromised, removal of the thermoplastic polymer additive from Met-L-X would potentially add performance stability during application as an explosion suppressant. During high-temperature aluminum flame propagation, agent decomposition volatiles likely dissociate and are less inclined to participate chemically in the combustion reaction inhibition. Reliance on physical inhibition and dilution mechanisms is key for effective suppression of deflagrations which display increasingly substantial reactivity.

5. CONCLUSIONS

Dust explosions induced by the ignition of reactive metal powders continue to present a substantial hazard within the metal handling and refining industries. High-rate injection of an inert agent material as the flame front begins to develop (i.e., active suppression) allows for deflagration extinction and effective mitigation of pressure growth within the protected enclosure volume. Inhibition of combustion propagation generally occurs via three routes: physical inhibition, chemical inhibition, and dilution of the preheat zone. However, due to characteristically intense severity and spontaneous burning mechanisms, the mitigation of metal powder deflagrations at moderate total suppressed pressures (relative to the overall design strength of the vessel) and at low agent concentrations remains challenging. As demonstrated through TGA/DSC analysis of fuel and fuel/agent mixtures, specific suppressant agent compositions appear to exhibit heightened inhibition performance as a result of greater overlap between the agent decomposition temperature range and fuel oxidation temperature range. Such overlap prompts increased chemical inhibition effectiveness, which acts as a direct supplement toward standard physical inhibition mechanisms. This study reviews recent metal dust suppression testing in a Fike Corporation's 1 m^3 sphere combustion chamber and evaluates the efficacy of multiple suppressant agents (sodium bicarbonate [SBC], sodium chloride [Met-L-X], and monoammonium phosphate [MAP]) for the mitigation of iron and aluminum powder deflagrations at suspended fuel concentrations of 2250 and 500 g/m^3, respectively.

DOI: 10.1021/acs.iecr.9b04021
Ind. Eng. Chem. Res. 2019, 58, 18007−18019

As predicted from thermal analytical studies, iron deflagration suppression experiments at a 70 mbarg set pressure and with MAP as the discharged suppressant agent yielded marginally lower reduced pressures (average TSP of 0.51 barg) relative to experiments with SBC (average TSP of 0.60 barg). According to TGA profiles for MAP, primary decomposition of the agent occurs directly atop the solid-phase combustion temperature range of iron powder. Compared to SBC and Met-L-X, whose decomposition temperatures exist either above or below the iron combustion temperature window, MAP offers deflagration mitigation by both physical and chemical means, absorbing the heat released via fuel oxidation and consuming free radicals which would otherwise prolong the combustion duration. Increased chemical inhibition effectiveness upon the use of MAP thus justifies the apparent reduction in TSP. If adopted commercially, it is recommended to modify the composition of the suppressant mixture (increased content of flow-promoting silica) in order to stimulate enhanced dispersion of the agent at higher target throw distances more representative of industrial application.

Aluminum deflagration suppression experiments at a 35 mbarg set pressure yielded TSPs greater than 1 barg for all agents tested. Relative to iron powder combustion (normally reactive), aluminum is considered a highly reactive metal and proved more difficult to suppress. Although Met-L-X was anticipated to demonstrate improved inhibition of aluminum combustion due to its high-temperature principal decomposition, suppression testing produced inconsistent results. Suppression of aluminum deflagration with Met-L-X yielded TSP as low as 1.33 barg and as high as 4.95 barg. Inspection of combustion chamber internals following Test Series 5 (Met-L-X, TSP = 4.95 barg) revealed a thin layer of material coating the top of a partially oxidized fuel/agent mixture. In this particular case, it is likely that the thermoplastic polymer additive within Met-L-X created ideal circumstances for a smoldering nest, which continued to burn and gradually generate pressure. As confirmed by the vessel pressure versus time profile for this test, the maximum suppressed pressure did not occur until several seconds after initiation of the event.

Chemical inhibition as a supplement to physical inhibition appeared to be less effective for the suppression of metal fuels with increasing reactivity. The influence of chemical inhibition on iron deflagration extinction was evident but marginal. Fuels such as aluminum display exceedingly high burning temperatures, which may lead to dissociation of decomposition volatiles that would normally impede combustion chemically or participate in dilution of the preheat zone. Greater metal fuel reactivity requires over-reliance on physical inhibition mechanisms. From a suppression system design standpoint, this translates to saturation of the combustion volume with an inert material at agent concentrations well beyond standard requirements. For suppression applications requiring high agent concentrations, the use of multiple smaller HRDs rather than a larger one is an effective design approach providing improved agent delivery rate and optimized agent throw distances. Maintaining appropriate response time through low-pressure activation set points allows the protection system an opportunity to extinguish the flame front before propagation accelerates to uncontrollable proportions. Combination venting with active suppression is also recommended for extremely reactive hazards to keep reduced pressures sufficiently below the enclosure design strength. Appropriate characterization of the hazard and conservative system design procedures are essential for proper protection of industrial processes conveying combustible metal dusts.

■ ASSOCIATED CONTENT

Supporting Information

The Supporting Information is available free of charge on the ACS Publications website at DOI: 10.1021/acs.iecr.9b04021.

Appendix A: mass loss profiles for 1:1 iron/agent mixtures; Appendix B: TGA and DSC profiles for inert materials; Appendix C: particle size analysis distribution profiles for fuels and agents; Appendix D: suppressant agent evolved gas analysis via mass spectrometry; Appendix E: open-air dispersion testing (PDF)

■ AUTHOR INFORMATION

Corresponding Author

*E-mail: nick.reding@fike.com. Tel: (913) 232-6294.

ORCID

Nicholas S. Reding: 0000-0002-3905-487X

Mark B. Shiflett: 0000-0002-8934-6192

Notes

The authors declare no competing financial interest.

■ ACKNOWLEDGMENTS

This study represents a collaborative effort between Fike Corporation and the University of Kansas. The authors acknowledge the assistance of NETZSCH (Mike Hsu; Melinda Tucker) and the University of Kansas in providing simultaneous thermal analysis (STA) for all fuel and agent samples. Additionally, the authors acknowledge the invaluable contributions of Fike Corporation's remote site testing facility staff and combustion test lab technicians in conducting open-air dispersion testing, fuel explosibility analysis, and 1 m^3 sphere active suppression experiments. The authors recognize the support of Fike Corporation in providing operational resources, continued funding of the test program, and consent to publish the results of this work.

■ REFERENCES

(1) U.S. Chemical Safety and Hazard Investigation Board. *Combustible Dust Hazard Study*, **2006**.

(2) U.S. Chemical Safety and Hazard Investigation Board. *Case Study No. 2011-3-I-WV*; AL Solutions, Inc.: New Cumberland, WV, 2010.

(3) U.S. Chemical Safety and Hazard Investigation Board. *Case Study No. 2011-4-I-TN*; Hoeganaes Corporation: Gallatin, TN, 2011.

(4) Li, G.; Yang, H.-X.; Yuan, C.-M.; Eckhoff, R. K. A catastrophic aluminum-alloy dust explosion in China. *J. Loss Prev. Process Ind.* **2016**, *39*, 121−130.

(5) Reding, N.; Shiflett, M. B. Metal Dust Explosion Hazards: A Technical Review. *Ind. Eng. Chem. Res.* **2018**, *57*, 11473−11482.

(6) Taveau, J. 17th Annual International Symposium; Mary Kay O'Connor Process Safety Center: College Station, TX, Oct 28−30, 2014; pp 594−606.

(7) Eckhoff, R. K. *Dust Explosions in the Process Industries*, 3rd ed.; Gulf Professional Publishing: Amsterdam, 2003.

(8) Reding, N.; Shiflett, M. B. Characterization of Thermal Stability and Heat Absorption for Suppressant Agent/Combustible Dust Mixtures via Thermogravimetric Analysis/Differential Scanning Calorimetry. *Ind. Eng. Chem. Res.* **2019**, *58*, 4674−4687.

(9) *CRC Handbook of Chemistry and Physics*, 86th ed.; Lide, D. R., Ed.; CRC Press: Boca Raton, FL, 2005.

(10) Taveau, J.; Vingerhoets, J.; Snoeys, J.; Going, J.; Farrell, T. Suppression of metal dust deflagrations. *J. Loss Prev. Process Ind.* **2015**, *36*, 244−251.
(11) Jiang, H.; Bi, M.; Gao, W.; Gan, B.; Zhang, D.; Zhang, Q. Inhibition of aluminum dust explosions by $NaHCO_3$ with different particle size distributions. *J. Hazard. Mater.* **2018**, *344*, 902−912.
(12) *NFPA 484: Standard for Combustible Metals*; National Fire Protection Association: Quincy, MA, 2015.
(13) Zalosh, R. Metal hydride fires and fire suppression agents. *J. Loss Prev. Process Ind.* **2008**, *21*, 214−221.
(14) Jiang, H.; Bi, M.; Li, B.; Gao, W. Inhibition of aluminum dust explosion by $NH_4H_2PO_4$ and $NaHCO_3$. In Proceedings of the Twelfth International Symposium on Hazards, Prevention and Mitigation of Industrial Explosions, Kansas City, MO, Aug 12−17, 2018.
(15) Chatrathi, K.; Going, J. Dust Deflagration Extinction. *Process Saf. Prog.* **2000**, *19*, 146−153.
(16) ASTM E1226, *Standard Test Method for Explosibility of Dust Clouds*; The American Society of Mechanic Engineers: West Conshohocken, PA, 2010.
(17) ISO 6184/1 *Explosion Protection System − Part 1: Determination of Explosion Indices of Combustible Dusts in Air*; International Organization for Standardization: Switzerland, 1985.

NOTE ADDED AFTER ASAP PUBLICATION

Due to a production error, this paper was published ASAP September 10, 2019, with the incorrect version of its Supporting Information document. The corrected version was reposted September 11, 2019.

DOI: 10.1021/acs.iecr.9b04021
Ind. Eng. Chem. Res. 2019, 58, 18007−18019